AUTOMATIC ALGORITHM FOR QUANTITATIVE PULSED PHASE THERMOGRAPHY CALCULATIONS

C. Ibarra-Castanedo, D. González and X. Maldague
Computer Vision and Systems Laboratory, Department of Electrical and Computer Engineering, Université Laval, Quebec City, QC, Canada.

Abstract: Pulsed Phase Thermography (PPT) has been successfully applied for defect detection purposes on a variety of materials. A great deal of work has been done to evaluate the potential of PPT for quantitative applications, using for instance statistical methods, Neural Networks or wavelets (Ibarra-Castanedo *et al.*, 2004). However, calibration requirements and lengthy computation subroutines, preclude their use on most NDT applications. A new inversion technique, based on phase delay data, has been recently proposed by the authors (Ibarra-Castanedo and Maldague, 2004a). Quantification is carried out by correlating the defect depth with its corresponding blind frequency, f_b, *i.e.* the frequency at which the defect becomes visible on the frequency spectra. Estimation of f_b is performed however using phase contrast calculations; as a result a non-defective zone on the sample surface is needed. As will be stressed, provided that thermal data is correctly sampled, phase profiles present a characteristic pattern that can be used on automatic f_b retrieval for a particular defect depth without defining a sound area.

Introduction: Pulsed Phase Thermography (PPT) combines interesting features from two older thermographic techniques, *i.e.* PPT is as rapid and easy to deploy as Pulse Thermograhy, and, after processing the thermal data, it provides phase delay images as Lock-In Thermography. It is well known that phase is less affected than thermal data by problems such as non-uniform heating, surface emissivity variations and non-planar surfaces. Accordingly, PPT is a safe and easy to deploy NDT technique, giving the possibility to rapidly inspect large and complex surfaces. Figure 1 summarizes the different steps involved on PPT. The specimen surface is first stimulated with a thermal pulse, *e.g.* using photographic flashes ❶, varying from a few seconds to several milliseconds depending on the thermal properties of the material being inspected. Once the pulse reaches the specimen ❷, the thermal front propagates through the material while the cool down process begins at the surface. The principle of defect detection is based on the fact that, at the surface, defective zones will be at higher or lower temperatures with respect to non-defective zones, depending on the thermal properties of both, the material and the defect. The temperature evolution on the surface is monitored using an infrared camera ❸. A thermal map of the surface, or thermogram, is recorded at regular time intervals. A 3D matrix is then formed, in reference to Figure 1, x and y coordinates are the horizontal and vertical pixel positions respectively, and the z-coordinate corresponds to the time evolution, in which the thermograms are separated Δt seconds from each other.

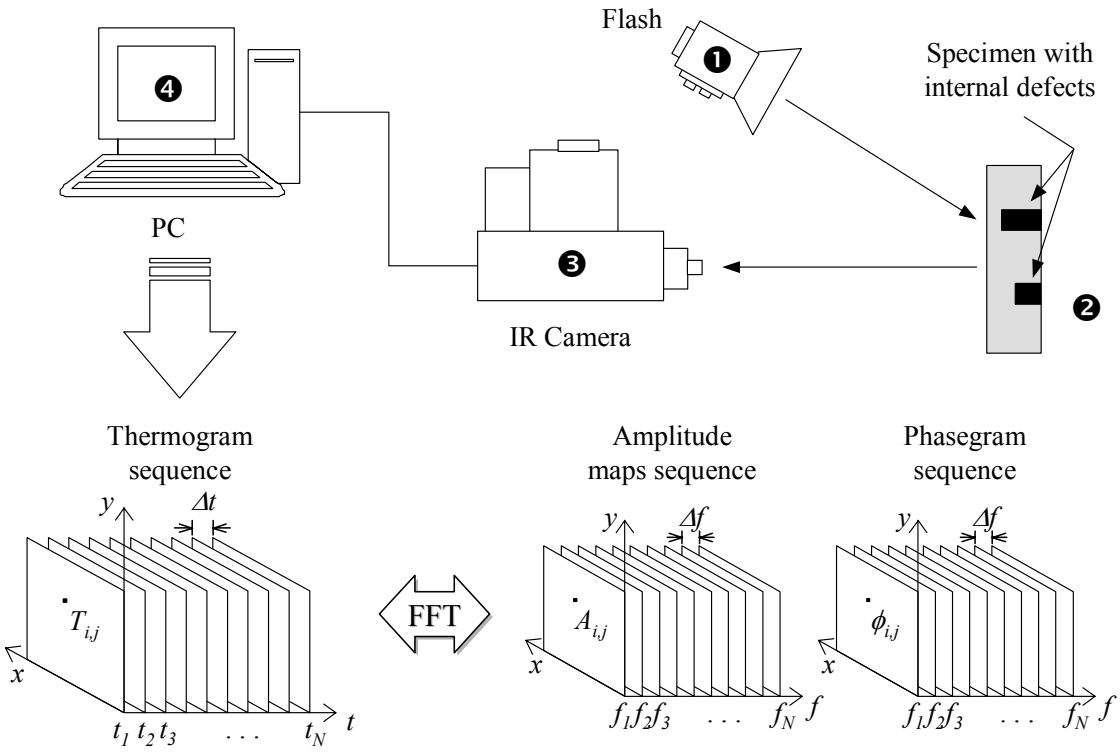

Figure 1. Data acquisition and processing by PPT.

The thermogram sequence is then processed ❹ using the Fourier Transform (Maldague and Marinetti, 1996):

$$F_n = \Delta t \sum_{k=0}^{N-1} T(k\Delta t) e^{-j2\pi nk/N} = \mathrm{Re}_n + \mathrm{Im}_n \tag{1}$$

where n designates the frequency increment (n=0,1,…N), Δt is the sampling interval and *Re* and *Im* are the real and the imaginary parts of the transform, respectively. The sampling interval Δt, is introduced in Eq. (1) as a scale factor in order to produce equivalence between the continuous and discrete Fourier Transforms (Brighman, 1974). For NDT applications, Eq. (1) is not practical due to lengthy computations. The Fast Fourier Transform (FFT) algorithm, available on software packages such as MatLab®, greatly reduces the computation timing and is therefore privileged. Real and imaginary parts of Eq. (1) can be use to calculate the amplitude and the phase of the transform:

$$A_n = \sqrt{\mathrm{Re}_n^2 + \mathrm{Im}_n^2} \quad \textit{and} \quad \phi_n = \tan^{-1}\left(\frac{\mathrm{Im}_n}{\mathrm{Re}_n}\right) \tag{2}$$

In order to perform the FFT on thermal data, the continuous temperature signal $T(t)$, is sampled at Δt time intervals and truncated with a rectangular window $w(t)$. Both $w(t)$ and Δt, or using its reciprocate the sampling frequency: f_s=1/ Δt, are strongly dependant on the thermal properties of the material being inspected. Appropriate selection of f_s primarily depends on the thermal properties of the specimen, but also in a variety of factors (Marinetti *et al.*, 1999) that complicate the development of analytical tools. The sampling theorem ($f_s \geq 2f_c$) should be respected for all defects present on the inspected specimen; the difficulty arises when trying to determine f_c. As a consequence, f_s is generally established empirically by taking some basic guidelines, *e.g.* high conductivity materials require a higher f_s to avoid loss of information (Ibarra-Castanedo and

Maldague, 2004b). In addition to be a function of the specimen's thermal properties, time-frequency duality plays an important role on *w(t)* size determination. Frequency resolution Δf, is directly linked to *w(t)* through the relationship (Brighman, 1974): $\Delta f=1/w(t)$. Contrary to f_s, for which analytical determination is difficult to perform, it is possible to predict the minimum *w(t)* size for a particular configuration using computer modeling. For instance, Marinetti *et al.* (1999) found that for a 20 mm CRFP specimen, the acquisition should last for at least 1000 s to correctly characterize a 6 mm thick defect. Similar studies are currently in progress in our laboratory. Indeed, this will help to the adequate selection of the acquisition parameters. Moreover, especial care must be taken to avoid exceeding the acquisition system's storage capabilities, given that the total number of recorded thermograms *N*, is a function of *w(t)* and f_s: $N=w(t)\cdot f_s$.

It is well known (Maldague and Couturier, 1997) that phase is practically unaltered by such problems as non-uniform heating, surface emissivity variations and the presence of non-planar surfaces that typically affect thermal signals. Therefore, there is a great interest in taking advantages of these characteristics for quantitative calculations. An inversion technique based on phase delay data has been recently proposed (Ibarra-Castanedo and Maldague, 2004a) and can be summarized using Figure 2.

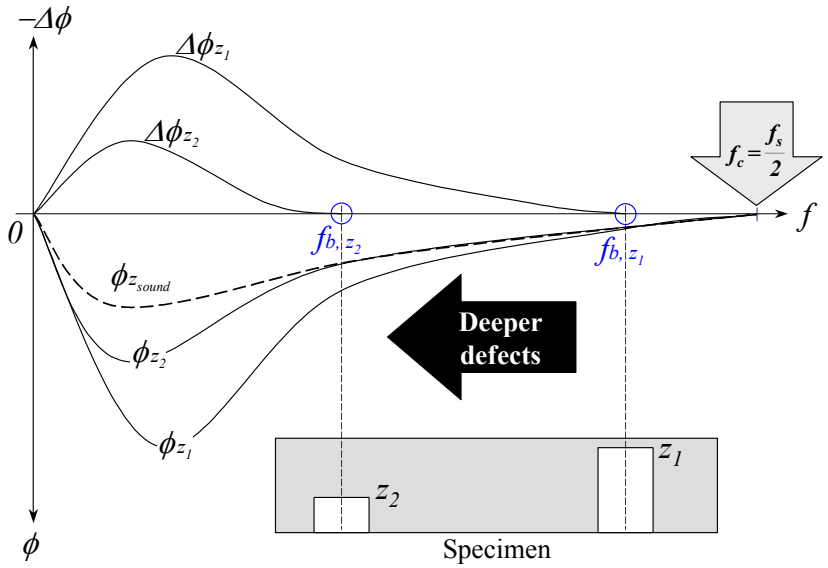

Figure 2. Depth retrieval with the phase contrast using the blind frequency.

Blind frequency values f_b, are calculated using the phase contrast definition (Sakagami *et al.*, 2002): $\Delta\phi=\phi_d-\phi_s$, by locating the frequency at which no significant phase contrast can be observed: $\Delta\phi<$threshold. Threshold values are established based on experimentation and depend on a variety of factors related to both the materials being inspected and the setup configuration (thermal properties, signal-to-noise ratio, etc.). From the diffusion length equation (Maldague, 2001): $\mu=(2\alpha/\omega)^{1/2}$, and the phase delay definition (Favro and Han, 1998): $\phi=z/\mu$, depth *z*, is related to f_b as follows:

$$z \propto \phi_s \sqrt{\frac{\alpha_s}{\pi\ f_b}} \tag{3}$$

where ϕ_s and α_s are the phase and the thermal diffusivity, respectively of the material being inspected, *i.e.* the sound area.

As previously explained, estimation of f_b requires a large enough *w(t)* in order to obtain an adequate frequency resolution, and that $f_s\geq 2f_c$ for all defects to be able to characterize them while keeping aliasing levels low. Hence, provided that these conditions are fulfilled, phase profiles for

a defect will exhibit a distinctive inflexion point at a particular frequency (*i.e.* the blind frequency), as illustrated in Fig. 2. For higher frequency components all phase profiles merge into a straight line, following the behavior of a non-defective zone. For lower frequencies, phase profiles behave differently according to their respective depth. Based on this fact, an automatic algorithm is proposed here to mathematically locate the frequency at which the separation occurs (*i.e.* the blind frequency) without performing phase contrast calculations. As a result, sound area definition is no longer needed. Basically, the algorithm estimates the curve slope by least squares regression, starting from the higher available frequency to a given frequency f_n. This frequency f_n, is progressively decreased (so more points are included in the regression at each time) and the slope is recalculated and compared to the previous value. The procedure is repeated up to a frequency at which the slope is considered to diverge from the non-defective slope. Precision parameters were established based on experimentation.

Results: Acquisition was carried out using a FPA infrared camera (Santa Barbara Focalplane SBF125, 3 to 5 mm), on a 320x256 pixel array with 14-bit resolution. Two high power flashes (Balcar FX 60), giving 6.4 kJ for 15 ms each, were used as heating sources. Thermographic data was analyzed with a PC (Pentium 4, 2 GB RAM) using MatLab® language from The MathWorks, Inc. Two Plexiglas® plates with flat-bottomed holes, PLEXI014 and PLEXI013 in Fig. 3a and b, were tested. Phase and phase contrast profiles for specimen PLEXI014 are presented in Fig. 4. Acquisition parameters are: f_s=0.28 Hz and $w(t)$=300 s, giving 86 thermograms to work with.

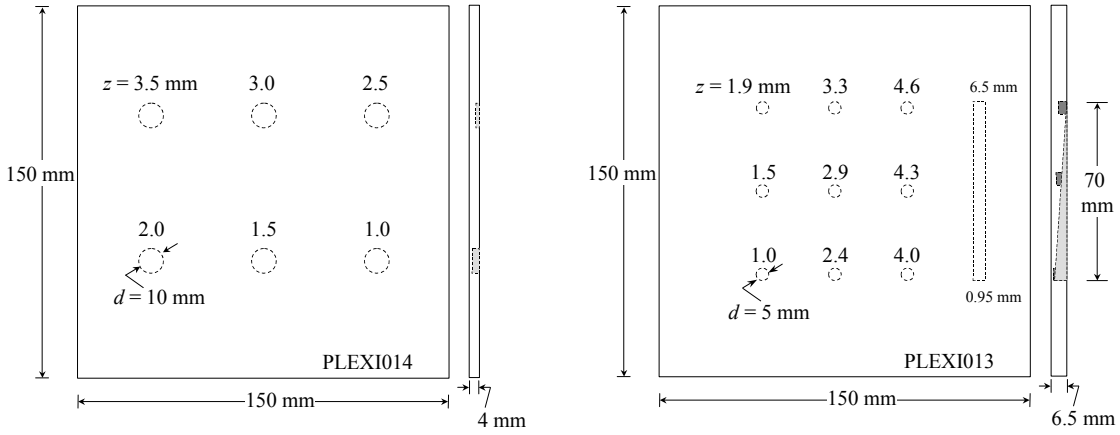

Figure 3. Studied specimens, (a) PLEXI014, (b) PLEXI013.

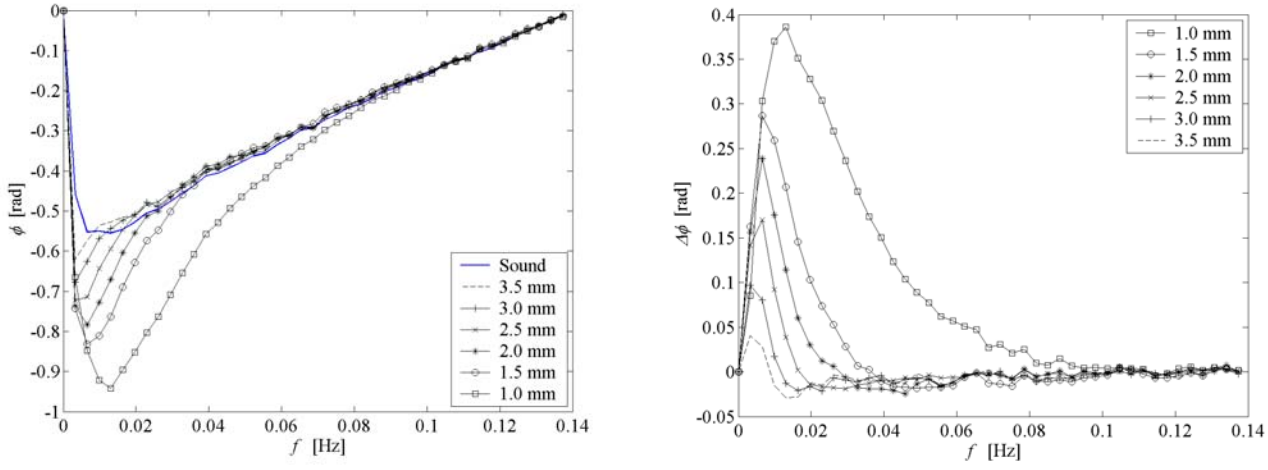

Figure 4. (a) Phase and (b) phase contrast profiles for specimen PLEXI014 in Fig. 3.

For sake of clarity, phase profiles for the defective zones in Fig. 4, are redrawn individually in Fig. 5. The corresponding depth for this profiles increases from the top left to the bottom right. A dotted blue line represents the slope for the non-defective part of the phase automatically calculated with the algorithm. Blind frequency values are marked with a blue circle for each case.

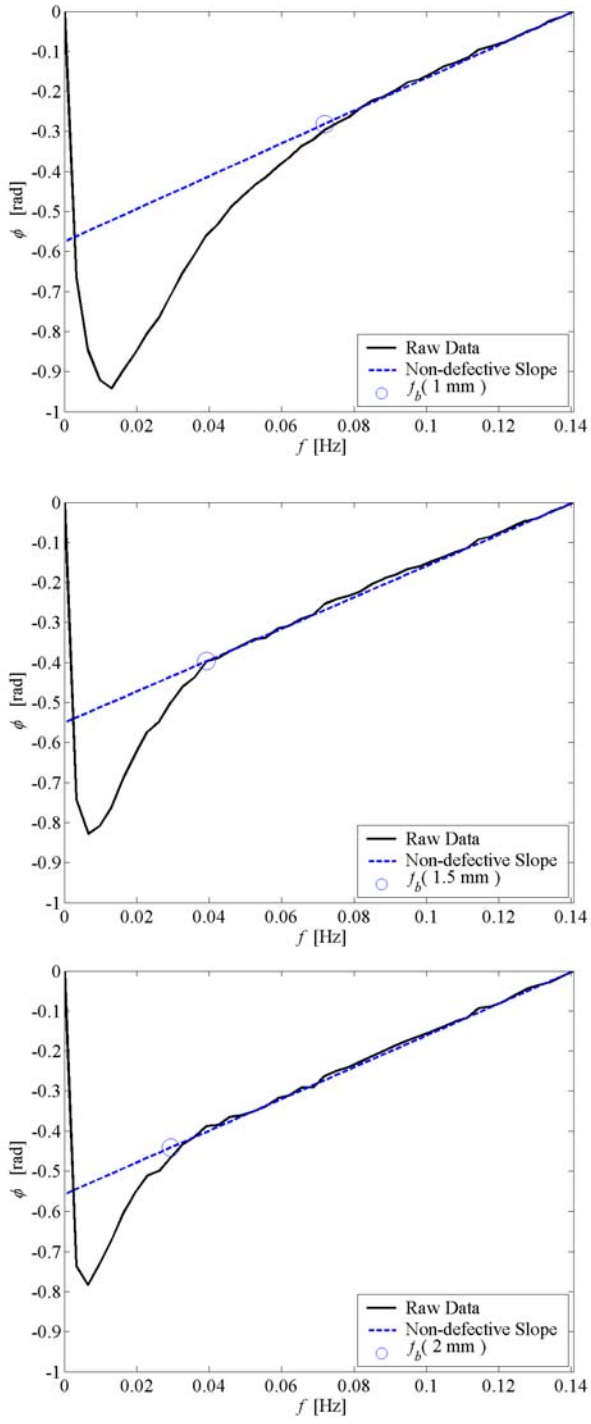

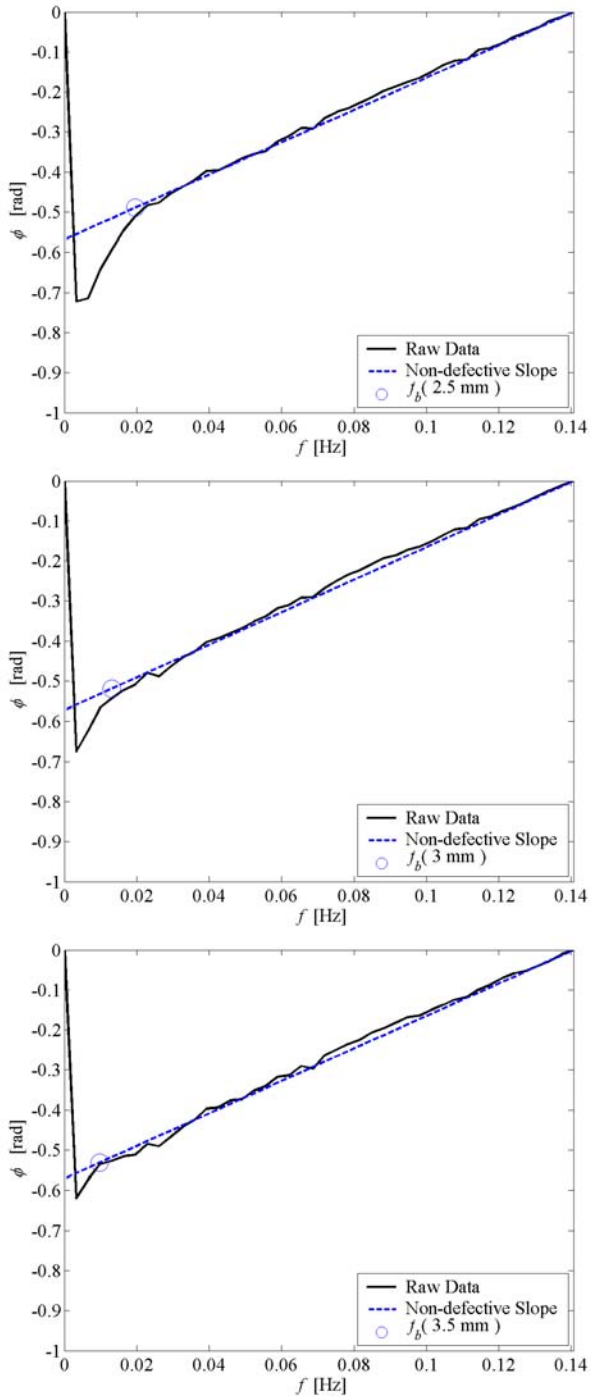

Figure 5. Phase profiles for the 6 defects on PLEXI014. The non-defective slope (dotted-line) and the estimated blind frequency (circle) are shown for each depth.

Results obtained from both, contrast calculations and automatic procedure, are presented in Fig. 6, as well as the location of the defects on the phasegram at f=0.0033Hz, corresponding to the minimum available frequency for this experience.

A similar analysis was applied to specimen PLEXI013 for the 3 shallowest flat-bottom holes and the shallowest part of the depth-varying slot (from 0.95 to 6.5 mm). Results are presented in Fig. 7 and 8.

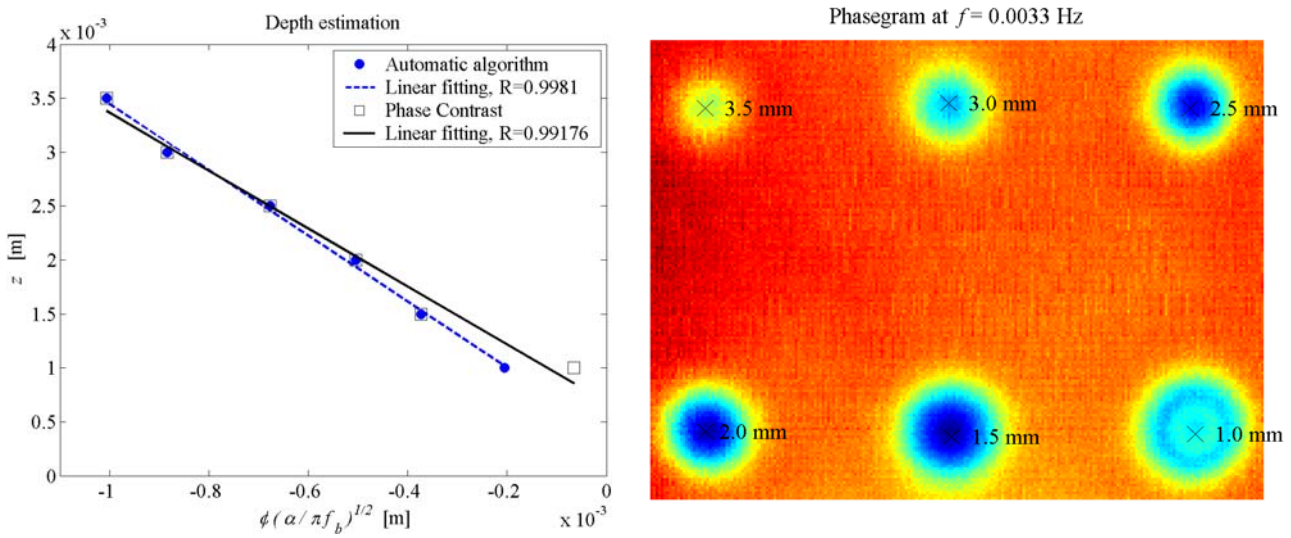

(a) **(b)**

Figure 6. PLEXI014 (a) z vs. f_b correlations using phase contrast and the proposed automatic algorithm, and (b) defect location in the phasegram at f=0.0033Hz (minimum available frequency).

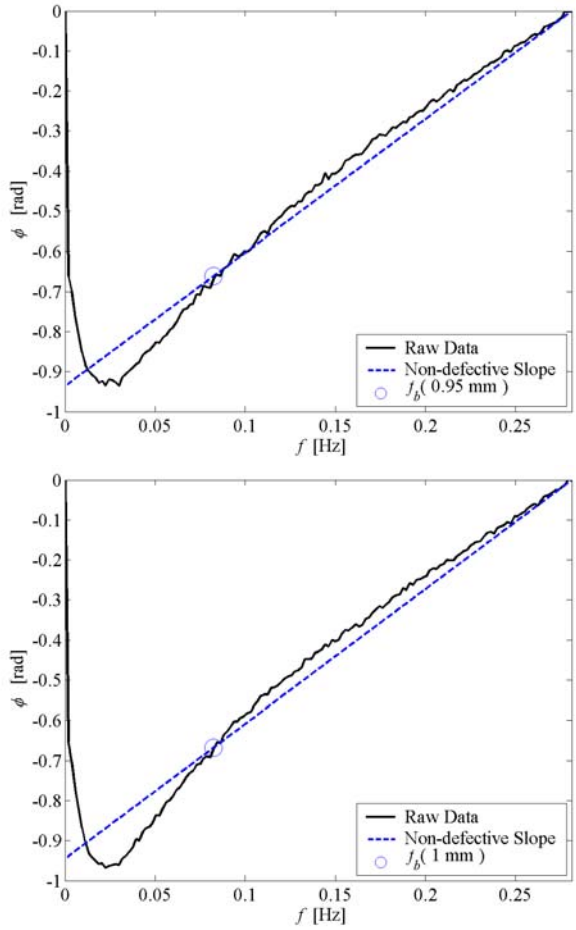

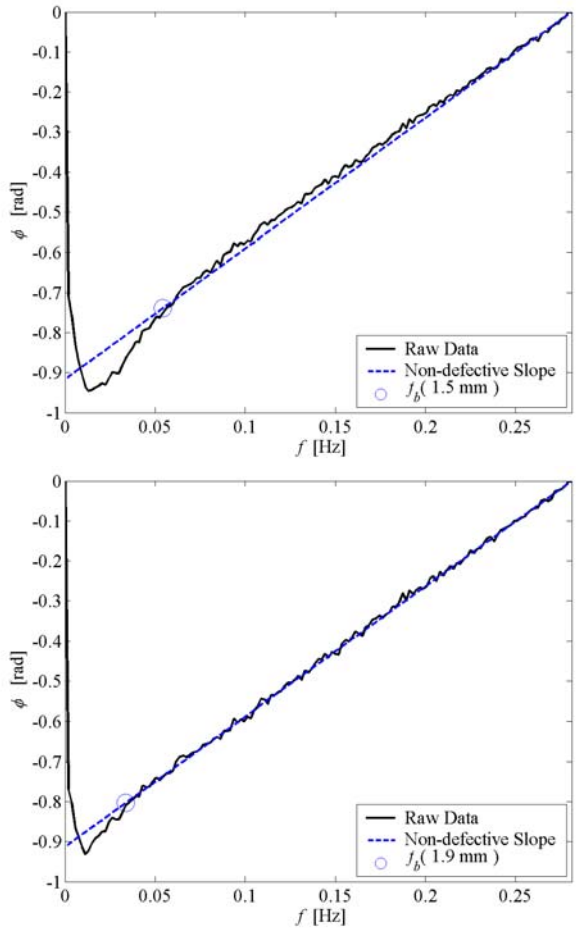

Figure 7. Phase profiles for 3 of the 9 defects on PLEXI013. The non-defective slope (dotted-line) and the estimated blind frequency (circle) are shown for each depth.

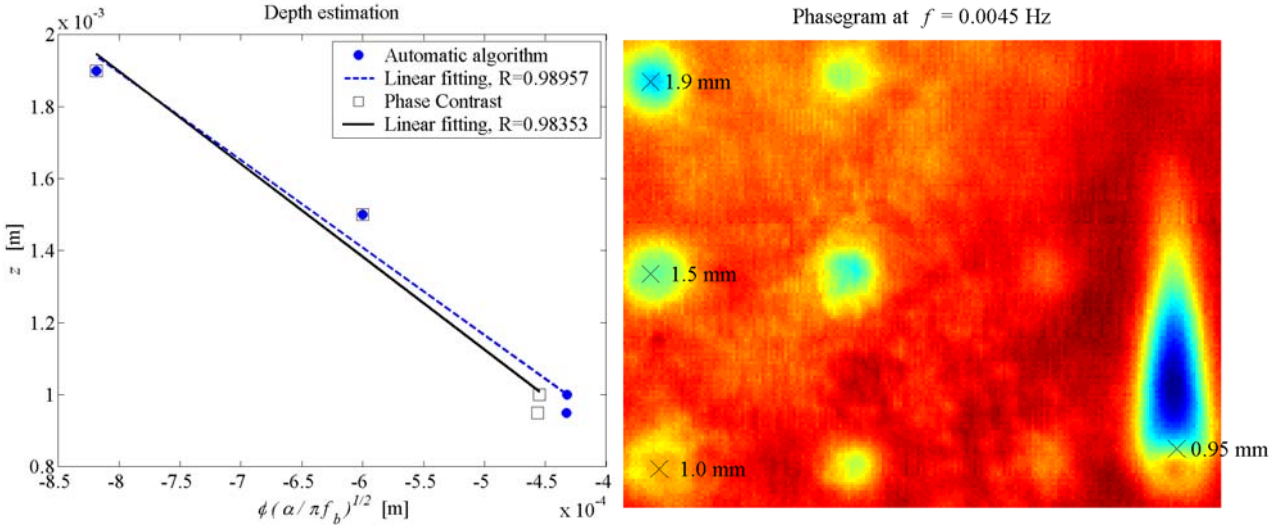

(a) **(b)**

Figure 7. PLEXI013 (a) z vs. f_b correlations using phase contrast and the proposed automatic algorithm, and (b) defect location in the phasegram at f=0.0045Hz (minimum available frequency).

Discussion: Contrast curves in Fig. 4 exhibit a pick value at low frequencies that should be dependant on the corresponding depth. However, there is not enough data in this case to correctly differentiate the depth on the curves. Blind frequency is a better choice. The relationship between z and f_b is no linear though. From Eq. (3), z should change proportionally to the square root of f_b. Phase profile for a specific sound area was used on contrast calculations in Fig. 4. As is well known (Martin *et al.*, 2003), results on sound area based operations show a great deal of variability depending on the selected sound region. Moreover, for non-academic specimens, a sound area is difficult if not impossible to locate.

As can be seen from Fig. 5, less data is available at low frequencies as depth increases. Therefore, error on the evaluation of f_b is expected to be higher for deeper defects. More precision can be achieved by further increasing the acquisition time, *i.e.* the size of *w(t)*. Of course, this will required additional memory space.

For 5 of the 6 defects on specimen PLEXI014 (shown in Fig. 3a), the estimated f_b values are exactly the same for both techniques, as can be see in Fig. 6. There is a difference only for the shallowest defect. The correlation coefficient is higher using the automatic algorithm. However, considering that depth is proportional to the square root of frequency, phase contrast calculations are closer to the expected behavior. Specimen PLEXI013 was more difficult to analyze, since the defects' diameter is smaller. Still, it was possible to detect and characterize 3 of the 9 different depths. Results from both techniques were also quite similar.

Conclusions: An automatic depth retrieval algorithm is proposed. The algorithm estimates the curve slope by least squares regression to iteratively locate the frequency value (*i.e.* the blind frequency), at which the slope for a defective phase profile diverges from the typical linear behavior for a non-defective region. The experimental results obtained on this study confirm that it is possible to automatically estimate the depth for a thick defect without using a sound area. Good agreement between the phase contrast method and the proposed algorithm was observed. In either case, adequate selection of *w(t)*, is of paramount importance. Analytical models for estimating the appropriate size of *w(t)* (currently in progress), will indeed help on the selection of the acquisition parameters. Equally important is the sampling rate f_s, which is related to the thermal properties. The higher sampling rate required by high conductivity materials is compensated in part by lower *w(t)* requirements.

References:

Brighman E. O. The Fast Fourier Transform, Englewood Cliffs, NJ, Prentice-Hall, Inc., 1974.

Favro L. D. and Han X. "Thermal Wave Materials Characterization and Thermal Wave Imaging," in Birnbaum G., Auld B. A. (eds.): *Sensing for Materials Characterization*, *Processing and Manufacuring, ASNT TONES,* vol. 1, p. 399-415, 1998.

Ibarra-Castanedo C., González D., Klein M. Pilla M., Vallerand S. and Maldague X. "Infrared Image Processing and Data Analysis," *Journal of Infrared Physics and Technology*, in press 2004.

Ibarra-Castanedo C. and Maldague X. "Defect Depth Retrieval from Pulsed Phase Thermographic Data on Plexiglas and Aluminum Samples," *Thermosense XXVI*, *Proc. SPIE*, vol. 5405, p. 348-356, Orlando, April 2004a.

Ibarra-Castanedo C. and Maldague X. "Pulsed Phase Thermography Reviewed," *J. QIRT*, in press 2004b.

Maldague X. and Couturier, J-P. "Review of Pulse Phase Infrared Thermography," *AITA 4*, Firenze (Italie), 15-16 septembre, 1997.

Maldague X. P. "Theory and Practice of Infrared Technology for Nondestructive Testing," John Wiley & Sons, N. Y., 2001.

Maldague X. P. and Marinetti S. "Pulse Phase Infrared Thermography," *J. Appl. Phys*., vol. 79, no. 5, p. 2694-2698, 1996.

Marinetti S., Plotnikov Y. A., Winfree W. P. and Braggiotti A. "Pulse Phase Thermography for Defect Detection and Visualization," *Proc. SPIE*, vol. 3586, p. 230-238, 1999.

Martin R. E., Gyekenyesi A. L. and Shepard S. M. “Interpreting the Results of Pulsed Thermography Data,” *Mater. Eval.*, vol. 61, no. 5, p. 611-616, 2003.